JET–P(98)82

D Testa et al

Interpretation of Measurement of Minority Hydrogen Isotope Ion Distribution Functions during Multispecies Ion Cyclotron Resonance Frequency Heating of Deuterium Plasmas in JET

JET–P(98)82

Interpretation of Measurements of Minority Hydrogen Isotope Ion Distribution Functions during Multispecies Ion Cyclotron Resonance Frequency Heating of Deuterium Plasmas in JET

D Testa[1,2], W G F Core, A Gondhalekar.

JET Joint Undertaking, Abingdon, Oxfordshire, OX14 3EA,
[1]Imperial College of Science, Technology and Medicine, London, UK.
[2]Present address: Plasma Science and Fusion Centre, Massachusetts Institute of Technology, Cambridge, MA02139, USA.

Preprint of a Paper to be submitted for publication in
Physics of Fluids B (Physics of Plasmas)

February 1999

ABSTRACT

We developed an iterative method for solving the hot-plasma dispersion relation and computing power deposition during multispecies minority Ion Cyclotron Resonance Frequency (ICRF) heating experiments. Here the distribution function of resonating ions becomes strongly anisotropic and significantly hotter than that of non-resonating particles. Therefore we have considered thermal and overlapping cyclotron harmonics effects for the interpretation of the measurements. We compute wave propagation and absorption for plasmas containing minority anisotropic fast ions using a complex perpendicular wavenumber in cylindrical geometry. In the minority heating scheme, we find that most of the ICRF power is coupled to minority ions and collisionless bulk ion heating is negligible when $T_{ibulk} \leq T_e$. However, if $T_{ibulk} > T_e$, then ICRF power couples also to the majority ions. We have successfully applied this method to the interpretation of measurements of hydrogen isotope ion distribution functions during multispecies minority ICRF heating of deuterium plasmas in JET.

P.A.C.S. numbers: 52.50.GJ, 52.35.HR, 52.55.FA, 52.65.FF

1. INTRODUCTION

Waves in the ion cyclotron range of frequencies (ICRF) have been effectively and reliably used to heat magnetically confined fusion plasmas. For the high power densities and long slowing-down times achieved in present-days experiments, the distribution function of resonating ions becomes strongly anisotropic, with a perpendicular temperature much higher than the parallel temperature, and significantly greater than that of non-resonating plasma species. These high energy anisotropic ion populations can significantly enhance the fusion yield above that of a thermal isotropic plasma for the same total energy content, and may also stabilise sawteeth and low frequency MHD modes [1,2]. Reliable measurements of the energy distribution function of such ions have also become well established [3,4].

Wave propagation and absorption is usually analysed using approximate expressions for the dielectric tensor and for the power deposition mechanisms [5,6,7]. Conversely, much greater effort has been made in incorporating into the analysis the correct geometry of the confining magnetic field. The most commonly used approximations for computing the dispersion relation are the *cold plasma* limit, which neglects thermal effects, and the *warm plasma* limit, which considers thermal corrections only to first order. The wavevector is treated as a real quantity, on the basis that its imaginary part is vanishingly small compared to the real part. Finite gyro-radius effects are generally considered only to second order in $k_\perp \rho_i << 1$. Thus cyclotron heating due to the counter-rotating component (E_-) of the wave electric field may not be properly accounted for, because the ratio between the co (E_+) and counter-rotating polarisation depends critically on $k_\perp \rho_i$ and $Im(k_\perp)$.

In JET, a number of sophisticated codes are used for interpretation of experiments with ICRF heating. They make use of the pertinent magnetic geometry, taking into account the D-shaped configuration of the JET tokamak and the presence of a poloidal magnetic field, thus allowing for a shift in the launched parallel wavenumber. Conversely, a simplified approach is used for the solution of the dispersion relation, which neglects minority ion species and uses the warm plasma approximation with a real perpendicular wavenumber.

These approximations may become inadequate to describe wave propagation and absorption in the presence of resonating ions since for them $k_\perp \rho_i \approx 1$ and $Im(k_\perp) << Re(k_\perp)$ does not hold true at the plasma edge, due to coupling of the launched fast magnetosonic waves to surface modes, in the ion cyclotron resonance layer, due to thermal effects of the resonating ions, and where mode conversion to Bernstein waves occurs. Thus cyclotron heating due to E_- as well as power absorption due to overlapping cyclotron harmonic effects can no longer be ignored. This mechanism is important since in a non-uniform magnetic field wave-particle interaction is a non-local process because for resonant ions $k_\perp \rho_i \approx 1$. The governing equations are coupled integro-differential equations for the components of the wave electric field $\{E_x, E_y, E_z\}$. Such a system has been formulated and solved for ICRF waves in fusion plasmas [8], and it has been shown [9,10] that an approximate method in which ICRF waves are described by a single second order differential equation is adequate as long as a sufficient number of overlapping harmonics is included in the computation. Here we follow this method.

Hot plasma theory allows us to fully analyse wave propagation and absorption for arbitrary ion gyro-radius, thus including implicitly the effect of overlapping cyclotron harmonics, by using a complex perpendicular wavenumber. We have developed a method for solving the hot plasma dispersion relation and computing power deposition in the ion cyclotron range of frequencies for plasmas containing minority anisotropic fast ions. The method uses measured thermal and non-thermal ion densities and temperatures and a complex wavenumber in cylindrical geometry to describe wave propagation and absorption in axisymmetric plasmas with a non-uniform magnetic field. Here we shall present details of such analysis.

For the minority ICRF heating scheme, in which resonating ions are present with different concentrations, a larger fraction of wave power is coupled to the minority ion species, and direct collisionless bulk ion heating is expected to be negligible for thermal plasmas with $T_e \geq T_{ib}$ (electron temperature greater than bulk ion temperature), so that $n_{ib}T_{ib} < n_f T_{\perp f}$ (bulk ion energy smaller than minority fast ion perpendicular energy) [11]. Conversely, injection of fast atoms into the plasma provides substantial collisional bulk ion heating. In this situation we show that cyclotron heating of majority ions becomes non-negligible for $T_{ib} \geq T_e$ and $n_{ib}T_{ib} > n_f T_{\perp f}$, thus reducing the ICRF power available to minority ions. These results agree quantitatively with measurements and modelling of the minority ion distribution functions.

For ICRF heating the power absorption mechanisms and the distribution function of resonant ions depend on each other, and much effort has been put into computing these two quanti-

ties self-consistently [7,12]. Fast anisotropic ions affect power deposition in two ways: *(a)* the parallel temperature determines the Doppler width of the ICRF resonance layer, modifying the absorption profile; *(b)* the perpendicular temperature determines the absorption strength, particularly for heating at frequencies other than the fundamental. However, minority resonant ion species have generally been neglected when computing the dispersion relation.

Our aim is to model and validate the measured minority fast ion distribution function in the plasma centre by analytically solving its evolution equation in velocity space, to demonstrate self-consistency between measurements and wave absorption and provide quantitative understanding of the experiments. Therefore we use a simplified magnetic configuration to avoid unnecessary numerical complications, however we consider the formal wave theory without simplifying the algebra required for its treatment to fully exploit its usefulness.

We use Neutral Particle Analyser (NPA) measurements [3,4] of the perpendicular distribution function of resonant ions in the energy range $0.3 \leq E(MeV) \leq 1.5$ as input for the calculations. We solve the hot-plasma ICRF dispersion relation in cylindrical geometry using a complex wavenumber, considering hydrogen isotope ion species with their respective concentrations and summing over an appropriate number of cyclotron harmonics. Using the dispersion relation we compute collisionless power partition between electrons and ions due to *Landau Damping* (LD), *Transit Time Magnetic Pumping* (TTMP) and *Cyclotron Damping* (CD). We compare the results of our calculations with Fokker-Planck (FP) modelling of the minority fast ion distribution function, magnetic measurements of the fast ion energy content and with a simple energy balance which neglects diffusion in velocity space and includes only losses due to ion-electron collisions, thus giving $W_i = n_i(T_{\perp i} + T_{||i}/2) = \rho_{ABS}\tau_S/2$ (absorbed power density times ion-electron slowing down time). We obtain quantitative agreement within the uncertainties of the measurements, usually of the order of *15%*.

This paper is organised as follows. In section 2 we discuss the dispersion relation and the power absorption mechanisms for ICRF waves. In section 3 we present the modelling of the velocity distribution function of ICRF heated high energy minority deuterons. In section 4 we apply this model to JET experiments with deuterium NBI and second harmonic ICRF heating of deuterium plasmas containing a background minority proton population. Finally, in section 5 we discuss our results and in section 6 we summarise our conclusions.

2. DISPERSION RELATION AND POWER ABSORPTION MECHANISMS IN THE ION CYCLOTRON RANGE OF FREQUENCIES

The ICRF dispersion relation is solved using cylindrical geometry for axisymmetric plasmas containing majority thermal isotropic and minority non-thermal anisotropic ion species. We consider Maxwellian distribution functions for thermal ions and electrons (with $T_{||} = T_{\perp} = T$), and bi-Maxwellians for fast ions (with $T_{||} < T_{\perp}$). The computation is carried over across the plasma minor radius for waves propagating from the low field side. We consider the antenna parameters

(wave angular frequency ω_{ICRF}, parallel wavenumber $k_{||}$ and ICRF heating power P_{ICRF}) and profiles for temperature, density and magnetic field as obtained in JET experiments with ICRF+NBI heating. The main difference between toroidal and cylindrical geometry is that the launched parallel wavenumber is kept constant across the plasma cross-section in the latter since there is no poloidal magnetic field. Conversely, toroidal tokamak geometry gives rise to a shift $k_{||}(x)=k_{||}(launched)\pm k_{\perp}(x)B_{\theta}(x)/\sqrt{2}B_{\phi}(x)$. Here B_{θ} and B_{ϕ} are the poloidal and toroidal components of the magnetic field and $x=r/a$ is the normalised minor radius, where $x=0$ corresponds to the plasma centre and $x=\pm 1$ corresponds to the plasma edge at the low (+1) and high (-1) magnetic field side.

We compute the dielectric tensor $\varepsilon(\omega,\boldsymbol{k})$ summing over contributions of hydrogen isotope ion species and electrons. In the ion cyclotron range of frequencies $|\varepsilon_{zz}|>>|\varepsilon_{ij}|$, and a simplified solution for the dispersion relation is obtained neglecting cross-field terms as [11,13]

$$\begin{pmatrix} \varepsilon_{xx}-n_{||}^2 & i\varepsilon_{xy} & \varepsilon_{xz}+n_{||}n_{\perp} \\ -i\varepsilon_{xy} & \varepsilon_{yy}-n_{||}^2-n_{\perp}^2 & i\varepsilon_{yz} \\ \varepsilon_{xz}+n_{||}n_{\perp} & -i\varepsilon_{yz} & \varepsilon_{zz}-n_{\perp}^2 \end{pmatrix} \xrightarrow{\omega\approx\Omega_i} \begin{pmatrix} \varepsilon_{xx}-n_{||}^2 & i\varepsilon_{xy} & 0 \\ -i\varepsilon_{xy} & \varepsilon_{yy}-n_{||}^2-n_{\perp}^2 & 0 \\ 0 & 0 & \varepsilon_{zz}-n_{\perp}^2 \end{pmatrix}.$$

Using the above distribution functions the conductivity tensor elements are given by

$$A_l = \left(1-\frac{k_{||}v_{0s}}{\omega}\right)Z_l - \frac{k_{||}v_{ths||}}{\omega}\left(\frac{T_{s\perp}}{T_{s||}}-1\right)W_l\,,$$

$$B_l = \frac{k_{\perp}v_{ths\perp}^2}{\Omega_s v_{ths||}}\left\{\frac{l\Omega}{\omega}\frac{v_{0s}v_{ths||}}{v_{ths\perp}^2}Z_l - \left[1-\frac{l\Omega_s}{\omega}\left(1-\frac{T_{s||}}{T_{s\perp}}\right)\right]W_l\right\},$$

$$C_l = -\frac{\omega-l\Omega_s}{k_{||}v_{ths||}}\left[1-\frac{l\Omega_s}{\omega}\left(1-\frac{T_{s||}}{T_{s\perp}}\right)\right]W_l\,,$$

$$\varepsilon_{ij} = \delta_{ij} + \sum_s \frac{\omega_{ps}^2 e^{-\lambda_s}}{\omega k_{||}v_{ths||}} \sum_{l=-\infty}^{\infty} \begin{pmatrix} \frac{l^2 I_l}{\lambda_s}A_l & il(I_l-I_l')A_l & lI_lB_l \\ -il(I_l-I_l')A_l & \left[\frac{l^2 I_l}{\lambda_s}+2\lambda_s(I_l-I_l')\right]A_l & -i(I_l-I_l')B_l \\ lI_lB_l & i(I_l-I_l')B_l & 2I_lC_l \end{pmatrix}.$$

Here s denotes the different plasma species, $\lambda=(k_{\perp}\rho)^2/2$ and $y_l=(\omega-l\Omega)/k_{||}v_{th}$, I_l and I'_l are modified Bessel functions of first kind and their derivative of argument λ, Z and W are plasma dispersion functions of argument y_l and δ_{ij} is the Kronecker's unitary tensor. For ICRF waves $\omega\approx\Omega_i<<\{\omega_{pe},|\Omega_e|\}$, therefore neglecting cyclotron resonances and using the small Larmor radius approximation $\lambda_e<<1$, the electron contribution to the conductivity tensor simplifies to

$$\varepsilon_{xx}^{(e)} = \frac{\omega_{pe}^2 \exp(-\lambda_e)}{\lambda_e \omega k_{||} \upsilon_{the}} \sum_{l=-\infty}^{\infty} l^2 I_l(\lambda_e) Z_e(y_l) \approx \frac{\omega_{pe}^2}{\Omega_e^2} + \frac{i\sqrt{\pi}\omega_{pe}^2}{\omega k_{||} \upsilon_{the}} \exp\left(-\frac{\Omega_e^2}{k_{||}^2 \upsilon_{the}^2}\right) = \varepsilon_{yy}^{(e)} ,$$

$$\varepsilon_{xy}^{(e)} = -\frac{\omega_{pe}^2 \exp(-\lambda_e)}{\omega k_{||} \upsilon_{the}} \sum_{l=-\infty}^{\infty} l\left[I_l(\lambda_e) - I_l'(\lambda_e)\right] Z_e(y_l) \approx \frac{\omega_{pe}^2}{\omega \Omega_e} ,$$

$$\varepsilon_{xz}^{(e)} = -\frac{k_\perp \omega_{pe}^2 \exp(-\lambda_e)}{k_{||} \omega \Omega_e \lambda_e} \sum_{l=-\infty}^{\infty} l I_l(\lambda_e) W_e(y_l) \approx -\frac{k_\perp \omega_{pe}^2}{k_{||} \Omega_e^2}\left[\frac{k_{||}^2 \upsilon_{the}^2}{\Omega_e^2} + \frac{i\sqrt{\pi}\Omega_e^2}{\omega k_{||} \upsilon_{the}} \exp\left(-\frac{\Omega_e^2}{k_{||}^2 \upsilon_{the}^2}\right)\right] ,$$

$$\varepsilon_{yz}^{(e)} = -\frac{k_\perp \omega_{pe}^2 \exp(-\lambda_e)}{k_{||} \omega \Omega_e} \sum_{l=-\infty}^{\infty} \left[I_l(\lambda_e) - I_l'(\lambda_e)\right] W_e(y_l) \approx \frac{k_\perp \omega_{pe}^2}{k_{||} \omega \Omega_e}\left[\frac{k_{||}^2 \upsilon_{the}^2}{\omega^2} - \frac{i\sqrt{\pi}\omega}{k_{||} \upsilon_{the}} \exp\left(-\frac{\omega^2}{k_{||}^2 \upsilon_{the}^2}\right)\right] ,$$

$$\varepsilon_{zz}^{(e)} = -\frac{2\omega_{pe}^2 \exp(-\lambda_e)}{\omega k_{||} \upsilon_{the}} \sum_{l=-\infty}^{\infty} I_l(\lambda_e) y_l W_e(y_l) \approx -\frac{\omega_{pe}^2}{\omega^2}\left[1 - \frac{2i\sqrt{\pi}\omega^3}{k_{||}^3 \upsilon_{the}^3} \exp\left(-\frac{\omega^2}{k_{||}^2 \upsilon_{the}^2}\right)\right] .$$

First we solve the *(2×2)* cold plasma dispersion relation for $n_\perp$. Here $n_{\perp C}$ is real, the conductivity tensor is independent of $n_{\perp C}$, and we obtain the second order equation

$$\varepsilon_\perp = 1 + \frac{\omega_{pe}^2}{\Omega_e^2} + \sum_j \frac{\omega_{pj}^2}{2\omega k_{||} \upsilon_{thj||}} \left(Z_1 + Z_{-1}\right)_j \ , \ \varepsilon_{xy0} = \frac{\omega_{pe}^2}{\omega \Omega_e} + \sum_j \frac{\omega_{pj}^2}{2\omega k_{||} \upsilon_{thj||}} \left(Z_1 - Z_{-1}\right)_j \ ,$$
$$\left(n_{||}^2 - \varepsilon_\perp\right) n_{\perp C}^2 + \left[\left(n_{||}^2 - \varepsilon_\perp\right)^2 - \varepsilon_{xy0}^2\right] = 0 \ . \qquad [1]$$

Here the reactive part of $\varepsilon_\perp$ and ε_{xy0} is neglected, the sum is intended over the ion species and $Z_{kj}=Z_j(y_k)$. Including now first order corrections in the temperature, and the reactive part of $\varepsilon_\perp$ and ε_{xy0}, we obtain the warm plasma dispersion relation as the fourth order equation

$$D = -\frac{3\upsilon_{the}^2}{8c^2} \frac{\omega^2 \omega_{pe}^2}{\Omega_e^4} + \sum_j \frac{\upsilon_{thj\perp}^2}{4c^2} \frac{\omega_{pj}^2}{\Omega_j^2}\left[\frac{\omega}{k_{||} \upsilon_{thj||}} \left(Z_2 + Z_{-2} - Z_1 - Z_{-1}\right)_j - \left(\frac{T_{j\perp}}{T_{j||}} - 1\right)\left(W_2 + W_{-2} - W_1 - W_{-1}\right)_j\right] ,$$

$$D n_{\perp W}^4 + \left(n_{||}^2 - \varepsilon_\perp\right) n_{\perp W}^2 + \left[\left(n_{||}^2 - \varepsilon_\perp\right)^2 - \varepsilon_{xy0}^2\right] = 0 \ . \qquad [2]$$

Here D is treated as a perturbation to the cold plasma dispersion relation: thus using $n_{\perp W}=n_{\perp C}(1+\delta)$ the solution of the warm plasma dispersion relation is obtained as

$$n_{\perp W} = n_{\perp C} - \frac{D n_{\perp C}^3}{2\left(\varepsilon_\perp - n_{||}^2\right)} \ . \qquad [3]$$

We obtain an initial guess for the complex hot plasma perpendicular refractive index $n_{\perp H}$ by computing the hot plasma *(2×2)* dielectric tensor using $n_{\perp C}$ and solving the second order dispersion relation

$$\left(n_{||}^2 - \varepsilon_{xx}\right)n_{\perp H}^2 + \left[\left(n_{||}^2 - \varepsilon_{xx}\right)\left(n_{||}^2 - \varepsilon_{yy}\right) - \varepsilon_{xy}^2\right] = 0 \ . \qquad [4]$$

An iterative method is applied to obtain convergence of the hot plasma solution to the desired accuracy: for computational stability we need to sum over a number of cyclotron harmonics proportional to the ion Larmor radius, $l_{BES}=c_0(A/Z^2)T_{\perp}(keV)$, where c_0 is a constant depending on the numerical accuracy. For JET deuterium plasmas corresponding to typical ICRF heating experiments containing two minority anisotropic fast ion species, protons and deuterons, with central parameters $n_{e0}=4x10^{19}m^{-3}$, $T_{e0}=T_{DBULK0}=10keV$, $n_p=n_{DFAST}=0.05n_e$, $T_{\perp DFAST0}=150keV$, $T_{\perp p0}=300keV$, $T_{||p,DFAST}=T_{\perp p,DFAST}/10$, we obtain convergence to the local solution of the hot-plasma dispersion relation with relative accuracy $\leq 10^{-8}$ using $c_0=0.5$ for ions and $c_0=0.2$ for electrons. Our approach corresponds to considering one cyclotron harmonic per *2keV* of ion temperature and *5keV* of electron temperature, consistent with the method proposed in [10].

Using the hot plasma dispersion relation we compute the fraction of power absorbed through LD+TTMP for electrons and ions using the *(3×3)* dielectric tensor, whereas to compute CD to ions it is again sufficient to retain only the *(2×2)* dielectric tensor. The *y*-component of the wave electric field $E_y(x)$ is computed locally [9,10] using the WKB approach to describe the propagation of a wave from the low field side to the plasma centre (the *x*-direction, whereas the magnetic field lies in the *z*-direction, corresponding to the toroidal axis)

$$\frac{d^2E_y(x)}{dx^2} + k_{\perp}^2(x)E_y(x) = 0 \xrightarrow{W.K.B.} E_y(x) = E_0\sqrt{\frac{k_{\perp}(1)}{k_{\perp}(x)}}\,exp\left(-i\int_1^x dx' k_{\perp}(x')\right). \qquad [5]$$

The normalisation constant E_0 is defined using the Poynting flux $S(x)$ at the plasma edge, close to the antenna location, $S(1)=c|n_{\perp}(1)E_y^2(1)|/8\pi=P_{ICRF}/A$, where A is the area of the poloidal surface intercepted by the wave beams. The *x*, *z*, left (E_+) and right (E_-) handed polarised components of the electric field are computed from E_y using the dispersion relations

$$\frac{E_x(x)}{E_y(x)} = -\frac{i\varepsilon_{xy}}{\varepsilon_{xx} - n_{||}^2} \ , \ \frac{E_z(x)}{E_y(x)} = \frac{i\varepsilon_{yz}(\varepsilon_{xx} - n_{||}^2) + i\varepsilon_{xy}(\varepsilon_{xz} + n_{||}n_{\perp})}{(\varepsilon_{xx} - n_{||}^2)(\varepsilon_{zz} - n_{\perp}^2) - (\varepsilon_{xz} + n_{||}n_{\perp})^2} \ ,$$

$$\frac{E_+(x)}{E_y(x)} = \frac{-i(\varepsilon_{yy} - \varepsilon_{xx} - n_{\perp}^2)}{2(\varepsilon_{xx} + \varepsilon_{xy} - n_{||}^2)} \ , \ \frac{E_-(x)}{E_y(x)} = \frac{i(\varepsilon_{yy} - \varepsilon_{xx} - n_{\perp}^2)}{2(\varepsilon_{xx} - \varepsilon_{xy} - n_{||}^2)} \ .$$

CD occurs with absorption of energy by particles that, in their own frame of reference, feel the wave electric field at their cyclotron frequency: the resonance condition is $\omega - k_{||}v_{th||} = l\Omega$. LD and

TTMP involve energy absorption by particles moving along the direction of the magnetic field with the parallel phase velocity of the wave: therefore the resonance condition is $\omega - k_{||} v_{th||} = 0$. For LD the force acting on the particles is $q\boldsymbol{E}$, for TTMP is $-\mu \nabla_{||} \boldsymbol{B}$, μ being the particle's magnetic moment. The power density absorbed due to collisionless wave-particle interaction is generally given as [13] $\rho = \omega Im(\mathbf{E}^* \bullet \varepsilon \bullet \mathbf{E})/8\pi$: the superscript * denotes complex conjugation. The power densities for LD+TTMP (cross terms must be retained because the two effects are coherent) and CD are [13]

$$\rho_{CD} = \frac{\omega}{8\pi}\left\{ | E_x |^2 \, Im(\varepsilon_{xx}) + | E_y |^2 \, Im(\varepsilon_{yy}) - 2\, Im\left(E_x^* E_y\right) Im(\varepsilon_{xy}) \right\}, \qquad [6]$$

$$\rho_{LD+TTMP} = \frac{\omega}{8\pi}\left\{ | E_z |^2 \, Im(\varepsilon_{zz}) + | E_y |^2 \, Im\left(\varepsilon_{yy}\right)_{l=0} - 2\, Im\left(E_y^* E_z\right) Im(\varepsilon_{yz}) + 2\, Re\left(E_x^* E_z\right) Im(\varepsilon_{xz}) \right\}$$

. [7]

A very interesting result is obtained for the ion populations using the small Larmor radius approximation $\lambda_i << 1$: in this limit the ion LD+TTMP is given in term of the ion CD as [13] $\rho^{(i)}_{LD+TTMP} \approx 4\lambda_i \rho^{(i)}_{CD} << \rho^{(i)}_{CD}$. An important consequence of this method is that we only need to normalise the wave electric field using the Poynting flux at the plasma edge to compute the power absorbed by different plasma species. This is due to the fact that allowing for $Im(k_\perp)$ intrinsically gives rise to power dissipation, for instance due to coupling of the launched fast wave to surface modes in the low density region at the plasma edge. Conversely, usual modelling of ICRF experiments in JET uses a real perpendicular wavenumber [12,14]. With this approach power dissipation occurs only due to the reactive part of the dielectric tensor computed for a real wavevector: parasitic losses at the plasma edge was included as *ad-hoc factor* to match experimental observations [7]. This procedure is no longer required when $Im(k_\perp)$ is explicitly considered in the analysis. For fast evaluation of the resonating ion distribution function, these conventional modelling use power deposition profiles tabulated from full-wave and ray-tracing calculations performed considering the actual D-shaped toroidal geometry of JET. With our approach, and although using a much simplified magnetic geometry, we obtain quantitative agreement with these much more sophisticated codes on power deposition profiles for ions and electrons.

3. MODELLING THE VELOCITY DISTRIBUTION FUNCTION OF ICRF HEATED HIGH ENERGY MINORITY DEUTERONS

High energy deuterium NBI combined with ICRF tuned to the 2nd harmonic of the deuterium cyclotron frequency ($\omega_{ICRF} = 2\Omega_D$) is routinely used in JET to heat the plasma. Following Stix, these NBI deuterons undergo ICRF-driven diffusion in velocity space, and a very significant

enhancement of the non-Maxwellian tail on their slowing down distribution function can be produced with energy well in excess of the injection energy [11,13].

The distribution function of NBI deuterons under the combined effects of Coulomb scattering on bulk deuterons and electrons and the resonant interaction with the ICRF wave field is described by a FP equation with quasi-linear diffusion operators. However, because ICRF diffusion acts preferentially on the perpendicular component of the velocity, the resulting tail is highly anisotropic. Thus a complete solution of the FP equation requires a full 2D velocity space approach and is not readily amenable to an analytic treatment. A number of numerical codes have been developed to solve the FP equation and other related problems: the PION code is used in JET for this purpose [7,12,14]. However, to compute the ICRF power absorbed by NBI deuterons, the energy transfer to the background plasma species, the fusion reactivity, and to interpret the measured resonant ion distribution functions only the lowest order or isotropic part of the solution is required.

We solve analytically the FP equation for NBI deuterons to lowest order using the cyclotron wave field characteristics given by the hot plasma dispersion relation, section 2. Finite Larmor radius effects and, when the 1st and 2nd cyclotron harmonic are both active, the effect of other resonating ions within the plasma are included. This is particularly important for deuterium NBI into a deuterium plasma with a minority proton concentration since $\Omega_p=2\Omega_D$. In this situation, due to finite Larmor radius effects, 2nd harmonic ICRF heating of bulk plasma deuterons is not expected to play a role in the heating of NBI deuterons and will be neglected.

The FP equation describing the collisional relaxation and the resonant interaction of the NBI ions with the ICRF wave field is given as [11,13]

$$\frac{\partial f}{\partial t} = S(t)\frac{\delta(\upsilon-\upsilon_0)}{\upsilon^2} + \frac{T}{m\upsilon^2\tau_S}\frac{\partial}{\partial\upsilon}\left(\upsilon^2\frac{\partial f}{\partial\upsilon}\right) + \frac{1}{\upsilon^2\tau_S}\frac{\partial}{\partial\upsilon}(\upsilon^3+\upsilon_C^3)f + \\ + \frac{1}{\upsilon^2}\frac{\partial}{\partial\upsilon}\left(\upsilon^2 D_{ICRF}\frac{\partial f}{\partial\upsilon}\right) \quad . \qquad [8]$$

Here f is the pitch-angle averaged distribution function, τ_S the Spitzer slowing-down time, T the effective plasma temperature, υ_C the critical velocity at which the ion-ion and ion electron collision frequencies are equal, $S(t)$ the NBI ion birth rate, υ_0 the NBI ion injection velocity:

$$f(\upsilon,t) = \frac{1}{2}\int_{-1}^{1}\partial\varsigma\, f(\upsilon,\varsigma,t)\ ,\ \tau_S = \frac{3mm_e\upsilon_{the}^3}{16\sqrt{\pi}Z^2e^4n_e\ln\Lambda}\ ,\ \upsilon_C^3 = \frac{3\sqrt{\pi}}{4}\frac{m_e}{m_i}\upsilon_{the}^3\ ,$$

$$T = T_e\left[1+\frac{n_p}{n_e}\left(\frac{m_p}{m_e}\right)^{1/2}\left(\frac{T_e}{T_i}\right)^{1/2}\left(1+\xi\right)^{-1/2}\right],\ \xi = \frac{\rho_P\tau_S}{3T_en_p}\ .$$

Here $\zeta=cos(\upsilon_{||}/\upsilon)$ is the pitch angle variable, Λ is the Coulomb scattering coefficient [15], ξ is the Stix parameter for 1st harmonic heating of the minority protons [11], which also describes the increase in electron temperature due to the presence of the high energy proton tail within the plasma, ρ_p is the surface averaged ICRF power density absorbed by the protons; n_p and n_e are the proton and electron density, m, m_p, and m_e are the NBI ion, proton and electron mass, T_e and T_i are the electron and bulk ion temperature, and υ_{the} is the electron thermal speed. The pitch-angle averaged ICRF diffusion coefficient is [11,13]

$$D_{ICRF}(\upsilon)=\sum_{l=-\infty}^{\infty}K_l\int_{-1}^{1}\partial\varsigma\left(1-\varsigma^2\right)\left|E_+J_{l-1}\left(\frac{k_\perp\upsilon}{\omega_{ICRF}}\sqrt{1-\varsigma^2}\right)+E_-J_{l+1}\left(\frac{k_\perp\upsilon}{\omega_{ICRF}}\sqrt{1-\varsigma^2}\right)\right|^2 . \quad [9]$$

Here E_+ and E_- are the left and right-handed polarised components of the wave electric field at $\omega_{ICRF}=2\Omega_D$, K_l is a constant determined from energy balance considerations. Using the ICRF power density absorbed by the resonant ions at the l^{th} harmonic ρ^l_{ABS}, K_l is obtained from

$$\rho^{(l)}_{ABS}=m\int_0^{\infty}\partial\upsilon f(\upsilon,t)\frac{\partial}{\partial\upsilon}\left[\upsilon^3 D_{ICRF}(\upsilon)\right] . \quad [10]$$

The procedure for solving the FP equation for the resonant ion distribution function, eq.[8], is well known. First we use the Laplace transform technique, defined by

$$f(\upsilon,t)=\frac{1}{2\pi i}\int_{c-i\infty}^{c+i\infty}dp f(\upsilon,p)exp(pt) ,$$

where $Re(c)>0$, to effect a reduction to a second order equation in the velocity variable which, with suitable initial conditions, is most conveniently solved using the Green function method. For the situation of NBI heating switched on before ICRF heating, the equation is solved with the initial condition of a slowing down NBI ion distribution function. Thus we obtain for K_l

$$K_l=\frac{\pi Z^2e^2}{8\mid l\mid m^2\Omega_D} . \quad [11]$$

Considering now the NBI heating to be switched on at time $t_0<0$, the ICRF heating at time $t=0$ and neglecting energy diffusion, the initial NBI ion distribution function is

$$f(\upsilon,t=0)=\frac{1}{\upsilon^3+\upsilon_C^3}S\left[-t_0-\frac{\tau_S}{3}ln\left(\frac{\upsilon_0^3+\upsilon_C^3}{\upsilon^3+\upsilon_C^3}\right)\right] . \quad [12]$$

Using the above procedure and the WKB method [16] to determine the Green functions, the NBI ion distribution function is obtained for subsequent times $t>0$. Therefore in the velocity range $\upsilon<\upsilon_0$, below the NBI injection energy, we have

$$f(\upsilon,t)=\frac{S\left[-t_0-\frac{\tau_S}{3}ln\left(\frac{\upsilon_0^3+\upsilon_C^3}{\upsilon_1^3+\upsilon_C^3}\right)\right]}{\upsilon_1^3+\upsilon_C^3}exp\left\{\int_{\upsilon}^{\upsilon 1}\frac{\left(3u^2+\frac{2T}{m}\right)du}{\frac{2Tu}{m}+\tau_S\left(u^2D_{ICRF}\right)'+u^3+\upsilon_C^3}\right\}+$$

$$+\frac{S\left[-t_0-\frac{\tau_S}{3}ln\left(\frac{\upsilon_0^3+\upsilon_C^3}{\upsilon_2^3+\upsilon_C^3}\right)\right]}{\upsilon_2^3+\upsilon_C^3}\left\{\frac{\frac{2T\upsilon_2}{m}+\tau_S\left(\upsilon_2^2D_{ICRF}\right)'+\upsilon_2^3+\upsilon_C^3}{\frac{2T\upsilon}{m}+\tau_S\left(\upsilon^2D_{ICRF}\right)'+\upsilon^3+\upsilon_C^3}\right\}\times$$

$$\times exp\left\{-\int_{\upsilon 2}^{\upsilon}\frac{\left(3u^2+\frac{2T}{m}\right)du}{\frac{2Tu}{m}+\tau_S\left(u^2D_{ICRF}\right)'+u^3+\upsilon_C^3}-\int_{\upsilon 2}^{\upsilon}\frac{\left(u^3+\upsilon_C^3\right)du}{u^2\left(\frac{T}{m}+\tau_S u^2D_{ICRF}\right)}\right\}+ \qquad [13]$$

$$+\frac{1}{\frac{2T\upsilon}{m}+\tau_S\left(\upsilon^2D_{ICRF}\right)'+\upsilon^3+\upsilon_C^3}S\left[-t-\int_{\upsilon}^{\upsilon 0}\frac{\tau_{SD}u^2du}{\frac{2Tu}{m}+\tau_S\left(u^2D_{ICRF}\right)'+u^3}\right]\times$$

$$\times exp\left\{-\int_{\upsilon}^{\upsilon 0}\frac{\tau_S\left(u^2D_{ICRF}\right)''du}{\frac{2Tu}{m}+\tau_S\left(u^2D_{ICRF}\right)'+u^3+\upsilon_C^3}\right\}$$

In the velocity range $\upsilon \geq \upsilon_0$, above the beam injection energy, we have

$$f(\upsilon,t)=\frac{S\left[-t_0-\frac{\tau_S}{3}ln\left(\frac{\upsilon_0^3+\upsilon_C^3}{\upsilon_1^3+\upsilon_C^3}\right)\right]}{\upsilon_1^3+\upsilon_C^3}\left\{\frac{\frac{2T\upsilon_1}{m}+\tau_S\left(\upsilon_1^2D_{ICRF}\right)'+\upsilon_1^3+\upsilon_C^3}{\frac{2T\upsilon}{m}+\tau_S\left(\upsilon^2D_{ICRF}\right)'+\upsilon^3+\upsilon_C^3}\right\}\times$$

$$\times exp\left\{-\int_{\upsilon 1}^{\upsilon}\frac{\left(3u^2+\frac{2T}{m}\right)du}{\frac{2Tu}{m}+\tau_S\left(u^2D_{ICRF}\right)'+u^3+\upsilon_C^3}-\int_{\upsilon 1}^{\upsilon}\frac{\left(u^3+\upsilon_C^3\right)du}{u^2\left(\frac{T}{m}+\tau_S u^2D_{ICRF}\right)}\right\}+ \qquad [14]$$

$$+\frac{1}{\frac{2T\upsilon}{m}+\tau_S\left(\upsilon^2D_{ICRF}\right)'+\upsilon^3+\upsilon_C^3}S\left[-t-\int_{\upsilon 0}^{\upsilon}\frac{\tau_S u^2du}{\frac{2Tu}{m}+\tau_S\left(u^2D_{ICRF}\right)'+u^3+\upsilon_C^3}\right]\times$$

$$\times exp\left\{-\int_{\upsilon 0}^{\upsilon}\frac{\left(3u^2+\frac{2T}{m}\right)du}{\frac{2Tu}{m}+\tau_S\left(u^2D_{ICRF}\right)'+u^3+\upsilon_C^3}-\int_{\upsilon 0}^{\upsilon}\frac{\left(u^3+\upsilon_C^3\right)du}{u^2\left(\frac{T}{m}+\tau_S u^2D_{ICRF}\right)}\right\}$$

Here $\upsilon_1 > \upsilon_2$ are respectively the solution of the equations

$$t - \tau_S \int_{\upsilon}^{\upsilon 1} \frac{u^2 du}{\frac{2Tu}{m} + \tau_S \left(u^2 D_{ICRF}\right)' + u^3 + \upsilon_C^3} = 0 \ , \qquad [15]$$

$$t - \tau_S \int_{\upsilon 2}^{\upsilon} \frac{u^2 du}{\frac{2Tu}{m} + \tau_S \left(u^2 D_{ICRF}\right)' + u^3 + \upsilon_C^3} = 0 \ . \qquad [16]$$

The superscript $'$ and $''$ denote derivative and double derivative with respect to the argument. Eqs.[13] and [14] with the subsidiary eqs.[15] and [16] define the general solution for the problem satisfying the initial condition of eq.[12]. To increase analytical tractability, we consider only heating at the 2nd harmonic: thus in the limit $|E_-/E_+| << 1$ the ICRF diffusion coefficient is

$$D_{ICRF} \approx 2K_2 |E_+|^2 \int_0^1 \frac{t^3 dt}{\sqrt{1-t^2}} J_1^2 \left(\frac{k_\perp \upsilon}{\omega_{ICRF}} t \right) . \qquad [17]$$

Now using the small Larmor radius approximation $J_1(x) \approx (x/2)^2$ and the definition of the Beta function $B(x,y) = \Gamma(x)\Gamma(y)/\Gamma(x+y)$ we obtain

$$D_{ICRF} \approx K_2 |E_+|^2 \left(\frac{k_\perp \upsilon}{2\omega_{ICRF}} \right)^2 B(3,1/2) = \frac{16}{15} K_2 |E_+|^2 \left(\frac{k_\perp \upsilon}{2\omega_{ICRF}} \right)^2 = D_2 \upsilon^2 \ . \qquad [18]$$

Now the integrals occurring in eqs.[15] and [16] are elementary and read for $\upsilon_{1,2}$ as

$$t - \frac{\tau_S}{3\left(1 + 4D_2\tau_S\right)} ln \left[\frac{(1 + 4D_2\tau_S)\upsilon_{1,2}^3 + \upsilon_C^3}{(1 + 4D_2\tau_S)\upsilon^3 + \upsilon_C^3} \right] = 0 \ .$$

Therefore in this approximation the effective NBI ion slowing down time is

$$t_S^{(EFF)} = \frac{\tau_S}{3\left(1 + 4D_2\tau_S\right)} ln \left[1 + (1 + 4D_2\tau_S) \frac{\upsilon_0^3}{\upsilon_C^3} \right] . \qquad [19]$$

We can now relate this pitch-angle averaged distribution function to its bi-Maxwellian form, corresponding to the NPA measurements discussed in [3,4,17], by noting that in the above derivation $\upsilon = (\upsilon_{||} + \upsilon_\perp)^{1/2}$ and $\zeta = cos(\upsilon_{||}/\upsilon)$. Thus we obtain

$$f(\upsilon_{||},\upsilon_{\perp}) = \frac{n}{\pi^{3/2}\upsilon_{th||}\upsilon_{th\perp}^2} exp\left(-\frac{\upsilon_{\perp}^2}{\upsilon_{th\perp}^2} - \frac{\upsilon_{||}^2}{\upsilon_{th||}^2}\right) =$$

$$= \frac{n}{\pi^{3/2}\upsilon_{th||}\upsilon_{th\perp}^2} exp\left[-\frac{\upsilon^2}{\upsilon_{th\perp}^2} - \frac{\upsilon^2\varsigma^2}{\upsilon_{th||}^2}\left(1-\frac{T_{||}}{T_{\perp}}\right)\right] = f(\upsilon,\varsigma)\ .$$

Now we can perform a straightforward integration over the pitch-angle variable ζ using the definition of the error function *erf(x)* and obtain for $T_{||} \neq T_{\perp}$

$$f(\upsilon) = \frac{1}{2}\int_{-1}^{1} \partial\varsigma f(\upsilon,\varsigma) = \frac{n}{2\pi\upsilon\upsilon_{th\perp}^2}\left(1-\frac{T_{||}}{T_{\perp}}\right)^{-1/2} exp\left(-\frac{\upsilon^2}{\upsilon_{th\perp}^2}\right) \mathrm{erf}\left[\frac{\upsilon}{\upsilon_{th||}}\left(1-\frac{T_{||}}{T_{\perp}}\right)^{1/2}\right]. \quad [20]$$

It is important to note here that the eqs.[12], [13] and [14] defining the NBI ion distribution function are no more Maxwellian in their energy dependence. Thus, in the applications of the above procedure we will use the NBI ion density as measured by the NPA [17] and introduce an effective tail temperature given at the mean energy of the measurements E_* by [4]

$$T_{EFF} = -T(E_*)\left\{\frac{d\left[\ln F(E)/\sqrt{E}\right]}{dE}\right\}\left(@\,E = E_*\right)\ . \quad [21]$$

4. ANALYSIS OF 2ND HARMONIC ICRF DEUTERIUM HEATING IN JET

As application of the results of the previous sections we consider the case of deuterium NBI into deuterium plasmas containing background minority protons. The ICRF system is tuned to deuterium 2nd harmonic heating in the plasma centre. This process is more effective for ions with larger Larmor radius, thus NBI deuterons are predominantly heated. The presence of a second resonant species, the minority protons, causes part of the ICRF power to be absorbed by the protons at the 1st cyclotron harmonic. Direct coupling of ICRF power to majority bulk deuterons is observed to be negligible for $T_{DBULK} \leq T_e$, but becomes significant for $T_{DBULK} > T_e$. Thus bulk ion heating predominantly occurs due to collisions with the NBI deuterons. Typical parameters for the experiments are central electron and bulk ion temperatures T_{e0}=5-10keV and T_{DBULK0}=5-30keV, central electron density $n_{e0}=3\text{-}5\times10^{19}m^{-3}$, thermal and NBI deuterium and proton concentration n_{DBULK}/n_e=0.8-0.9, n_{DFAST}/n_e=0.01-0.1 and n_p/n_e=0.03-0.15, ICRF power P_{ICRF}=3-5MW, NBI power P_{NBI}=10-20MW, beam injection energy E_0=80/140keV, toroidal magnetic field on axis $B_{\phi 0}$=2-3.4T, plasma current I_{ϕ}=2-4MA. NBI heating is usually switched on 0.5-1s before ICRF heating.

The system of eqs.[12]-[16] and [20] is solved using the JET ICRF antenna parameters and the measured ion and electron distribution functions as input quantities for the calculations of the dispersion relation and power absorption. Thus we obtain $k_{\perp}$ and the ICRF power coupled

to different plasma species, which enables us to compute D_{ICRF} and thus $f(\upsilon)$ and the effective perpendicular tail temperature T_{EFF}. We then compute the total fast ion energy content using a collisional energy balance, which includes only losses due to ion-electron collisions [4,17]

$$W_{FAST} = \sum_{FAST} \int dV_{PLASMA} \frac{\rho_{ABS}\tau_S}{2} = \sum_{FAST} \int dV_{PLASMA} \left[nT_{\perp} \left(1 + \frac{T_{||}}{2T_{\perp}} \right) \right]_{FAST} = W_{MAG} \ . \quad [22]$$

Here the sum is intended over all resonant ion species, $\rho_{ABS}=\rho_{CD}+\rho_{LD+TTMP}$ and V_{PLASMA} is the plasma volume. We compare W_{FAST} with the total energy content of the measured distribution functions and the magnetic measurement W_{MAG}, T_{EFF} with the temperature $T_{\perp FAST}$ inferred from W_{FAST} and W_{MAG} using the measured fast ion densities and with the NPA measurements of $T_{\perp NPA}$ in the energy range $0.3 \le E(MeV) \le 1.5$, which typically lies 2-5 times above the typical $T_{\perp NPA}$ for the ICRF heating experiments reported here.

In fig.1 we show the effect of wave induced diffusion on NBI deuterons for a model situation: we use $k_{\perp}=(25,i5)m^{-1}$ and the ICRF power coupled to protons and NBI deuterons $P_p=0.5MW$ and $P_{DFAST}=3MW$. We obtain a hot tail in the deuterium distribution function: the effective temperature $T_{EFF}=\langle m\upsilon^2/2\rangle$ of NBI deuterons increases from $T_{EFF}=77keV$ for $P_{DFAST}=0$ to $T_{EFF}=129keV$ for $P_{DFAST}=3MW$, with a energy enhancement factor $\langle \Delta E \rangle \approx 0.68$ defined by

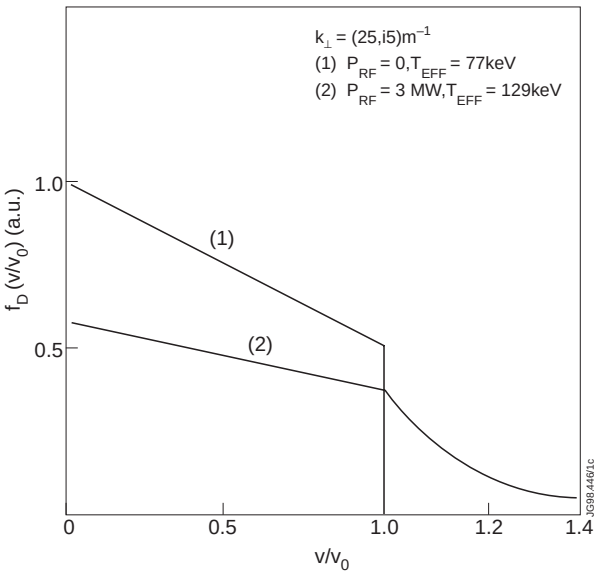

Fig.1: The NBI deuterium distribution function in the plasma centre as function of the normalised injection velocity υ/υ_0. We consider here a model situation with $n_{e0}=4.5\times10^{19}m^{-3}$, $n_{DBULK}/n_e=0.94$, $n_p/n_e=0.03=n_{DFAST}/n_e$, $T_{e0}=7keV$, $T_{DBULK0}=15keV$, $E_0=140keV$, $P_{NBI}=10MW$, $P_{DFAST}=0$-$3MW$, using the solution of the hot-plasma dispersion relation $k_{\perp}=(25,i5)m^{-1}$. NBI heating is switched on 1s before ICRF heating. The effective tail temperature $T_{EFF}=\langle m\upsilon^2/2\rangle$ increases from $T_{EFF}=77keV$ for $P_{DFAST}=0$ to $T_{EFF}=129keV$ for $P_{DFAST}=3MW$, with a significant enhancement of the total energy content of the NBI deuterons, $\langle \Delta E \rangle \approx 0.68$.

$$\langle \Delta E \rangle = \frac{\langle T_{EFF}(P_{DFAST}=3MW) \rangle - \langle T_{EFF}(P_{DFAST}=0) \rangle}{\langle T_{EFF}(P_{DFAST}=0) \rangle} \approx 0.68 \ . \quad [23]$$

Our calculations contain $T_{||}$ for NBI deuterons as a free parameter. Using wave dispersion, we obtain energy equi-partition as $T_{||}/T_{\perp} \approx (k_{||}/k_{\perp})^2$: $T_{\perp}$ is directly measured by the NPA, $k_{||}$ is given by the antenna and $k_{\perp}$ is the solution of the dispersion relation, which implicitly depends on $T_{||}$ and $T_{\perp}$. We determine $T_{||}$ for NBI deuterons through self-consistent solution of the dispersion relation: we use the above initial guess for $T_{||}$, solve the dispersion relation, obtain $k_{\perp}$, update $T_{||}$, and iterate until we find convergence with the prescribed residue for $k_{\perp}$. We typically

need 2-3 iterations to obtain the *true* $T_{||}$ with a residue $\leq 10^{-8}$ and $|T_{||}(guess)-T_{||}(true)|/T_{||}(true)<5\%$.

A more difficult problem is related to the basic fact that $\Omega_p=2\Omega_D$, and 2nd harmonic deuterium heating coincides with 1st harmonic proton heating. We model the proton population with a bi-Maxwellian distribution function using independent measurements of n_p/n_D, and energy equi-partition for the proton parallel and perpendicular temperatures. Thus we obtain [17]

$$T_{\perp p} = T_{DBULK} + \sqrt{\frac{m_D}{m_p}}\,\frac{W_e}{W_{DBULK}+W_{DFAST}}\,T_{\perp DFAST}\ ,\ T_{||p} = \frac{k_{||}^2}{k_{\perp}^2}\,T_{\perp p}\ .$$

Here W_e is the electron energy density. These results are critical for our calculations, since the magnetic measurement W_{MAG} of the fast ion perpendicular energy content gives the sum over ion species. Thus we have a very important test of this procedure by comparing W_{MAG} with $W_{\perp p}+W_{\perp DFAST}$: a discrepancy indicates lack of accuracy in our modelling of the proton population.

We neither use a-priori power deposition profiles, as in conventional JET modelling [12,14], nor ad-hoc factors to normalise the total absorbed power to the ICRF power. We determine power tunnelling through the low-density region at the plasma edge, local power absorption and power partition between ions and electrons using the species contribution to the hot plasma conductivity tensor and to $Im(k_{\perp})$. Thus we have two more important tests of our procedure: *(a)* the power computed must not exceed the input power; and *(b)* CD must occur in the ICRF resonance layer, as determined by the wave frequency and Doppler width.

We present results for three pulses, illustrating typical experiments with deuterium NBI and central ICRF heating at $\omega_{ICRF}=\Omega_p=2\Omega_D$. Pulse #40305 exemplifies *polychromatic* heating: the antennae are used at different frequencies with dipole phasing $0\pi0\pi$, to give a spreading in the resonance position of the order of the Doppler width, and $k_{||}\approx 7m^{-1}$. This scheme gives broader power deposition profiles, to reduce the minority resonant ion tail temperature and increase bulk ion and electron heating. Pulse #40474 is an example of *monochromatic* heating with dipole phasing: a single frequency is used, to give centrally localised minority ion heating. Pulse #40554 is an example of *monochromatic* heating with mixed phasing $\pi/2\text{-}0\pi0$, to give $k_{||}\approx(3\text{-}7)m^{-1}$. This scheme aims at producing non-inductive electron current drive to modify the plasma current profile, since now the launched wave spectrum is toroidally asymmetric.

Figs.2, 3 and 4 show the main central parameters for the above pulses: the magnetic field and plasma current are constant during the ICRF+NBI additional heating phase. The electron density increases due to NBI fuelling and the bulk deuterium temperature becomes larger than the electron temperature due to collisions with NBI deuterons. The measured NBI deuterium density and temperature are constant after the initial transient phase of the heating for #40305 and #40474, and are slowly changing in time for #40554. Therefore we consider satisfied the steady-state approximation used for modelling the NBI deuterium distribution function.

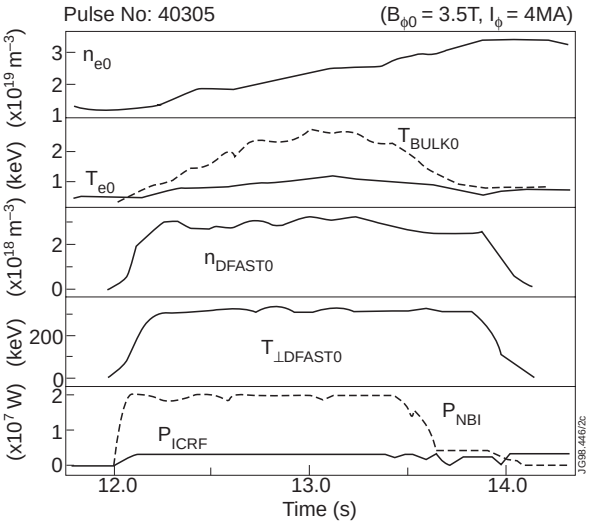

Fig.2: Main central parameters for JET pulse #40305: the toroidal magnetic field $B_{\phi 0}$ and the plasma current I_ϕ are constant during the additional heating phase. The background plasma is slowly varying: therefore we consider satisfied the steady-state approximation for modelling the NBI deuterium distribution function. The bulk ion temperature increases over the electron temperature due to NBI heating. The NBI deuterium temperature is sustained after termination of ICRF heating for $\tau \approx 0.4$s., consistent with the slowing-down time $\tau_D \approx 1.1$s.

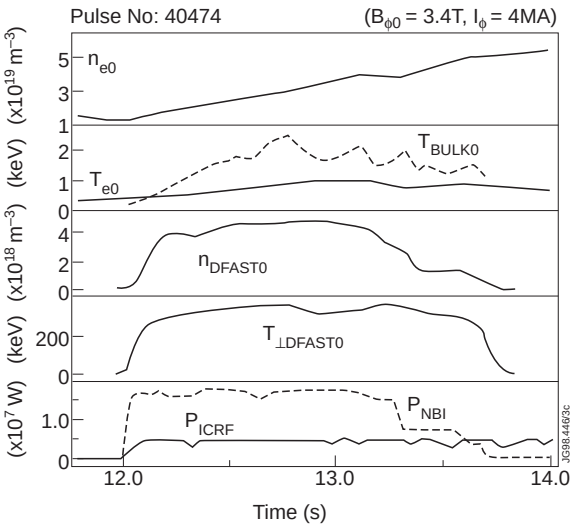

Fig.3: Main central parameters for JET pulse #40474: the toroidal magnetic field $B_{\phi 0}$ and plasma current I_ϕ are constant during the NBI+ICRF heating phase. The background plasma is slowly varying with time: therefore we consider satisfied the steady-state approximation for modelling the NBI deuterium distribution function. The bulk ion temperature increases over T_e due to NBI heating. The NBI deuterium temperature is sustained after termination of ICRF heating for $\tau \approx 0.4$s.: this is consistent with the measured slowing-down time $\tau_D \approx 1.0$s.

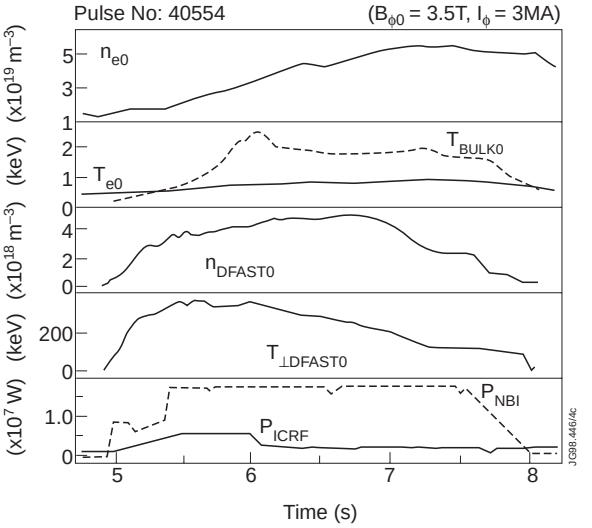

Fig.4: Main central parameters for JET pulse #40554: the toroidal magnetic field $B_{\phi 0}$ and plasma current I_ϕ are constant during the additional heating phase. The background plasma is slowly changing with time after the initial transient phase: therefore we consider satisfied the steady-state approximation for modelling the NBI deuterium distribution function. The bulk ion temperature increases over T_e due to NBI heating. The NBI deuterium temperature slowly decreases following reduction of ICRF power from 6MW to 2MW at t=6: this is very well related to a much longer slowing-down time $\tau_D \approx 1.8$s.

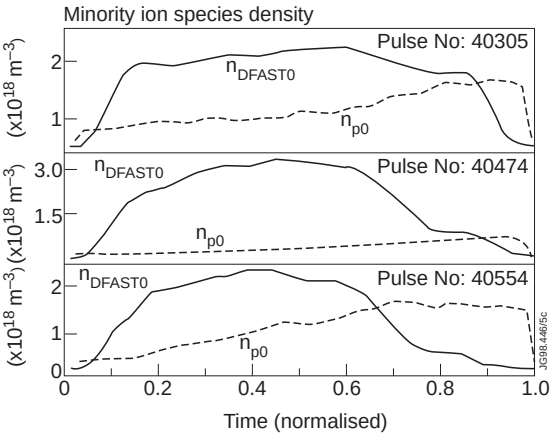

Fig.5: Central NBI deuterium and proton density for the pulses analysed here as function of normalised time: heating starts at $\tau=0$ and ends at $\tau=1$. NBI fuelling sustains n_{DFAST0}, and after the initial transient phase n_{p0} steadily increases over n_{DFAST0} due to recycling from the walls, particularly relevant when NBI heating is switched-on or off. For #40305 and #40554 the fast deuteron and proton densities are comparable during the main heating phase, whereas for #40474 $n_{DFAST0} >> n_{p0}$ due to higher ICRF power, P_{ICRF}=5MW compared to P_{ICRF}=2MW.

Fig.5 shows the minority proton n_{p0} and NBI deuteron density n_{DFAST0} in the plasma centre for the pulses considered here: we use a normalised time scale, where $\tau=0$ marks the beginning of the NBI+ICRF heating phase and $\tau=1$ its end. NBI determines n_{DFAST0}, whereas n_{p0} is largely sustained by recycling from the walls. Power partition between CD at 1st and 2nd harmonic is determined for the same Larmor radius by n_{DFAST0}/n_{p0}: higher n_{p0}, less the CD on deuterons.

Figs.6, 7 and 8 show (for #40305, #40474 and #40554) the power deposition profiles for CD and LD+TTMP on majority and minority ions and electrons as function of *r/a*, computed using the dispersion relation. We average the measurements over *50ms* and consider three different time-points during the heating phase: *(a)* at the end of the initial transient phase, *(b)* during the steady-state phase, *(c)* immediately before the final ramp-down of the heating.

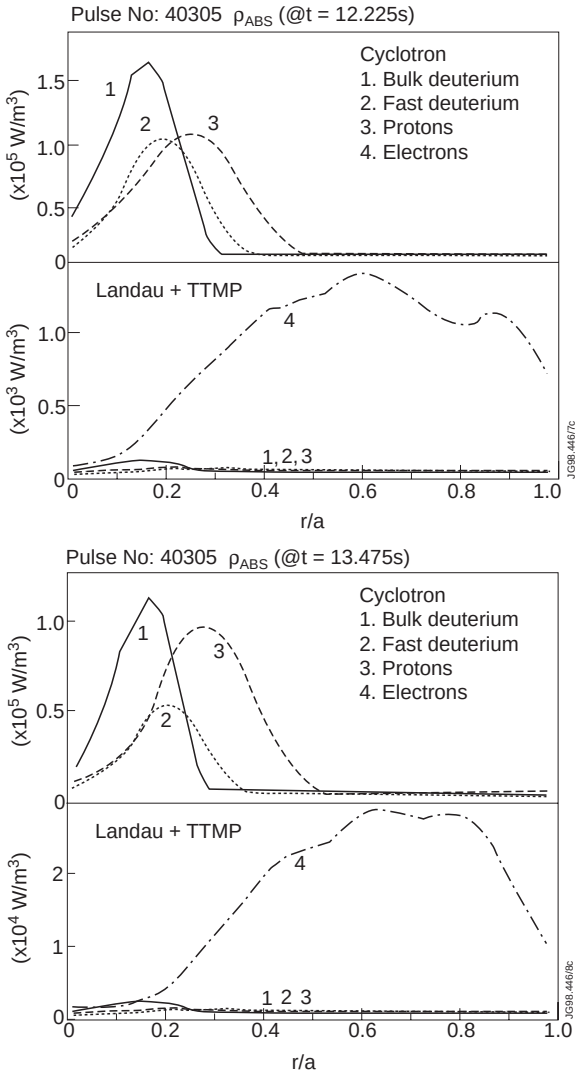

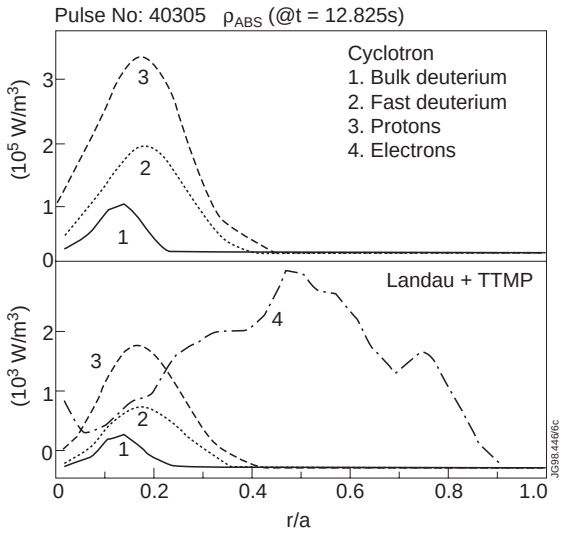

Fig.6: Direct collisionless polychromatic ICRF heating for pulse #40305 as function of r/a. We compute power partition between plasma species and deposition profiles from wave dispersion. Strong influx of hydrogen due to recycling from the walls at the beginning and end of the heating phase determines CD onto minority protons and deuterons. In fig.6a we present our results for t=12.225, at the end of the initial transient phase; fig.6b for t=12.825, during the steady-state phase; fig.6c for t=13.475, immediately before the final ramp-down of the heating. The electron heating profile broadens following the raise in T_e due to collisions with injected and ICRF-heated fast ions, and its magnitude increases due to NBI fuelling. The first peak at r/a≈0.5 can be attributed to ELD, the second peak at r/a≈0.8 to TTMP.

Our calculations show some general features of the heating in these experiments. Ion LD is negligible compared to cyclotron heating, since the wave phase velocity is much larger than the ion parallel thermal speed. This is a well-known theoretical result: it further validates our numerical procedure and verifies the assumption that parallel ion heating essentially occurs due

to collisions and energy equi-partition. At the beginning of the heating phase power absorption due to CD on the fast ion populations (NBI deuterons and protons) is the dominant process, but when $T_{DBULK} \geq T_e$ direct collisionless bulk ion heating appears to prevail. This result can be misleading: power absorption increases almost linearly with density for different ion species with same Larmor radius, being proportional to the conductivity tensor elements. Conversely, the increase in electron heating over ion heating can be directly related to the increase in electron temperature due to collisions with injected and ICRF-heated fast ions.

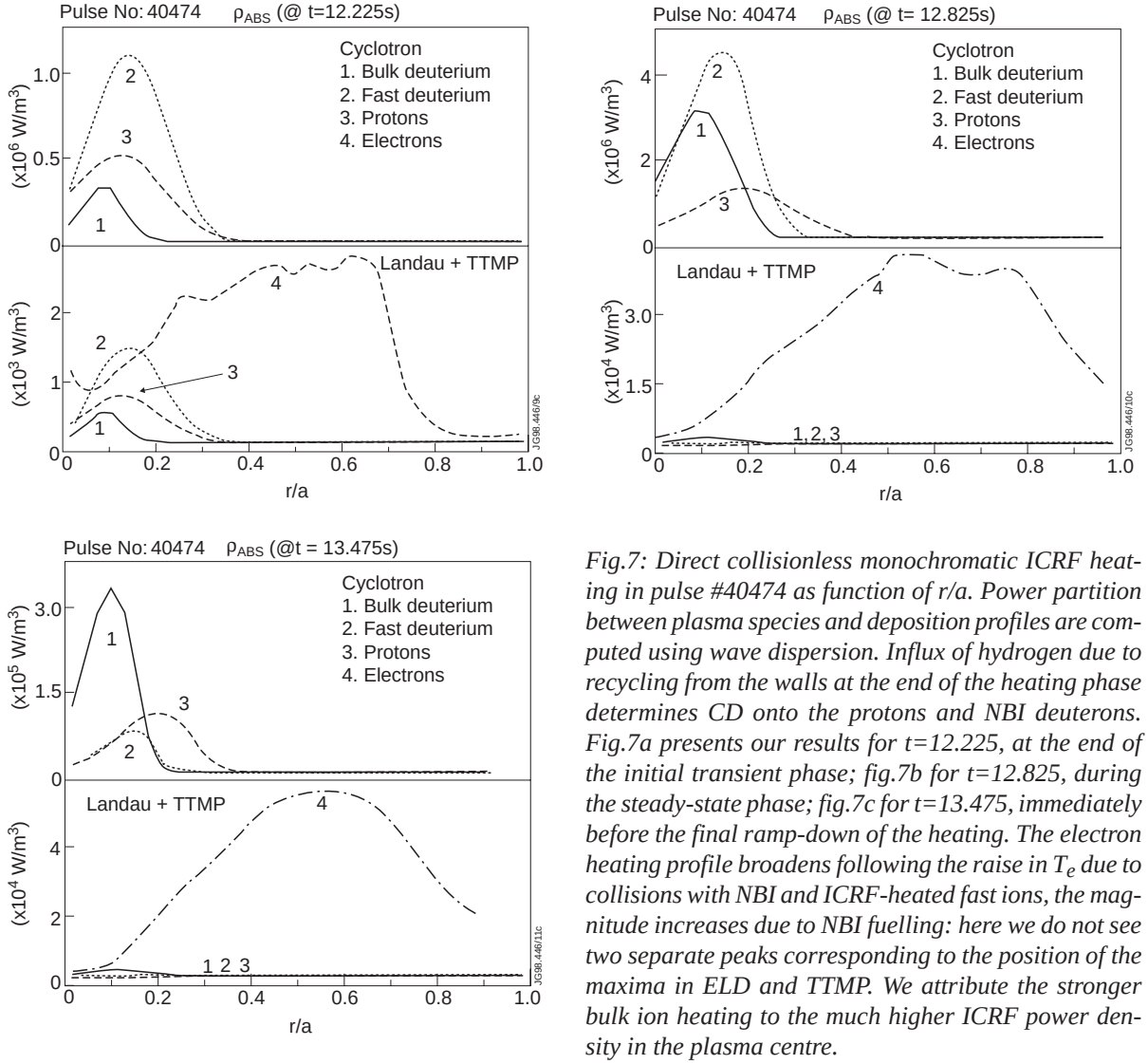

Fig.7: Direct collisionless monochromatic ICRF heating in pulse #40474 as function of r/a. Power partition between plasma species and deposition profiles are computed using wave dispersion. Influx of hydrogen due to recycling from the walls at the end of the heating phase determines CD onto the protons and NBI deuterons. Fig.7a presents our results for t=12.225, at the end of the initial transient phase; fig.7b for t=12.825, during the steady-state phase; fig.7c for t=13.475, immediately before the final ramp-down of the heating. The electron heating profile broadens following the raise in T_e due to collisions with NBI and ICRF-heated fast ions, the magnitude increases due to NBI fuelling: here we do not see two separate peaks corresponding to the position of the maxima in ELD and TTMP. We attribute the stronger bulk ion heating to the much higher ICRF power density in the plasma centre.

We notice that for polychromatic heating, as shown in fig.6 for #40305, the CD deposition profile is broader than that obtained for monochromatic heating, as shown in fig.7 for #40474 and fig.8 for #40554. The peak in ion CD is in the ICRF resonance layer: its location depends on $Im(\varepsilon_{xx}+\varepsilon_{yy})|E_+|^2$. This factor varies for different ion species: for polychromatic heating we expect the shape of the CD deposition profile for protons and deuterons to be similar but not exactly overlapping, with a shift depending on wave frequency and ion species temperature [12]. The electron deposition profile depends on LD $\approx Im(\varepsilon_{zz})|E_{||}|^2$ and TTMP $\approx Im(\varepsilon_{yz})|E_y|^2$: for

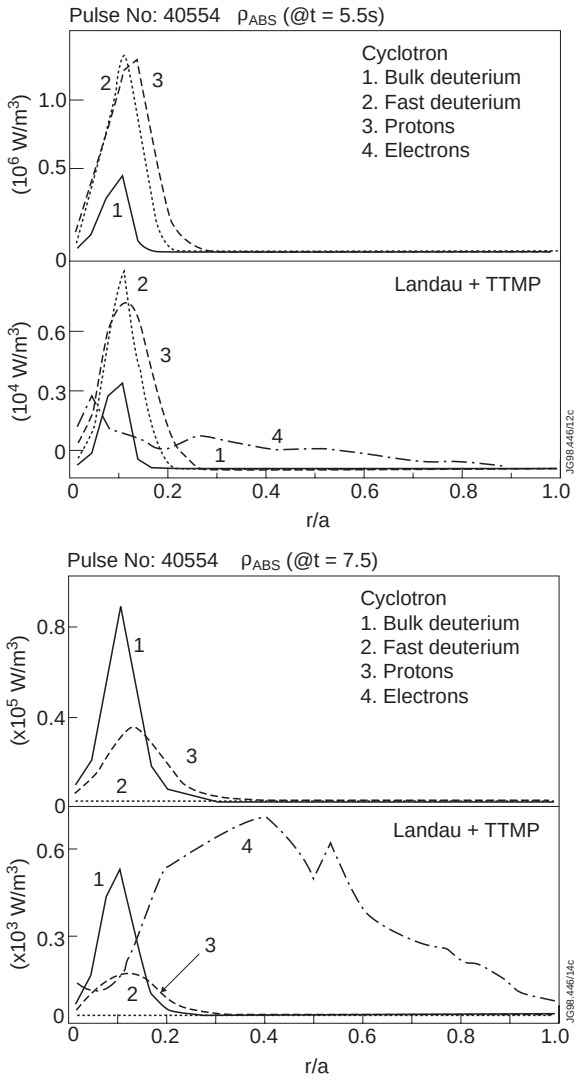

Fig.8: Direct collisionless monochromatic ICRF heating in pulse #40554 as function of r/a. Power partition between ions and electrons and deposition profiles are computed using wave dispersion. Influx of hydrogen due to recycling from the walls occurs after t=6, determining the strong increase of CD onto the protons over that onto NBI deuterons. Fig.8a presents our results for t=5.5, at the end of the initial transient phase; fig.8b for t=6.5, during the steady-state phase; fig.8c for t=7.5, immediately before the final ramp-down of the heating. Contrary to #40474, where we have a similar wave power density, at the beginning of the heating phase bulk ion heating is negligible due to the lower ion temperature. The electron heating profile shows two clear peaks, at r/a≈0.4 for ELD, and at r/a≈0.6 for TTMP.

large electron temperature the position of their maxima may not be identical, although we expect a broad gaussian shape peaked near the centre of the poloidal cross-section [12]. Our results agree with these predictions even if we use cylindrical geometry for the magnetic field, which is much simplified with respect to the D-shaped toroidal geometry of JET. Thus we are confident in their accuracy and ability to model the NBI deuterium distribution function.

We see for #40305 in fig.6 that CD on NBI deuterons and protons are comparable only for the steady-state heating phase, CD on protons being larger otherwise. This result depends on the fact that the proton density is larger than the NBI deuterium density at the beginning and end of the heating phase due to recycling from the walls, and during the initial transient phase wave power is coupled preferentially to 1st harmonic heating. We see for #40474 in fig.7 that CD on NBI deuterons is larger than CD on protons but at the end of the heating phase, where we observe strong influx of hydrogen due to recycling from the walls. For #40554 (different antennae phasing) we see in fig.8 that the electron absorption profile has two clear peaks, whereas for #40305 and #40474 we see a quite broad gaussian shape. We attribute the peak at *r/a≈0.3* to wave-driven current carrying electrons, localised closer to the plasma centre since in resonance

with the fraction of the wave spectrum launched with $\pi/2$ phasing. The electrons in resonance with the waves launched with dipole phasing produce the peak at $r/a \approx 0.5\text{-}0.6$.

Figs.9, 10 and 11 show power partition between ions and electrons for #40305, #40474 and #40554. We notice two important results: *(a)* the total power P_{CALC} (including Bernstein wave heating) computed from wave dispersion accounts for almost exactly the ICRF input power, the difference being $<10\%$; *(b)* some power $P_{LOST}/P_{ICRF} \leq 5\%$ is lost due to coupling to surface modes in the low-density region at $r/a>0.9$. We notice that CD on the protons is the dominant absorption process for the initial transient phase of the heating: collisionless bulk ion heating is important only for $T_{DBULK}>T_e$. Similarly, electron heating increases significantly following the increase in T_e due to collisions with fast ions: at the most, $\approx 25\%$ of wave power is directly coupled to electrons due to the combination of LD and TTMP. In PION, loss of power at the plasma edge is used in modelling similar experiments to reconcile the calculations with global and local measurements such as plasma energy and neutron rate, without a clear explanation being proposed [7]. Here we show that this loss process is a typical feature of the hot-plasma ICRF dispersion relation due to coupling of the launched fast magnetosonic wave to surface modes in the low-density region at $r/a>0.9$. Using the hot-plasma dielectric tensor, a second solution is possible in the ion cyclotron range of frequencies with the perpendicular refractive

$P_e \approx 0.5$MW	$P_{DBULK} \approx 0.8$MW	$P_{DFAST} \approx 0.5$MW	$P_p \approx 1.0$MW
$P_e/P_{ICRF} \approx 17\%$	$P_{DBULK}/P_{ICRF} \approx 27\%$	$P_{DFAST}/P_{ICRF} \approx 17\%$	$P_p/P_{ICRF} \approx 33\%$

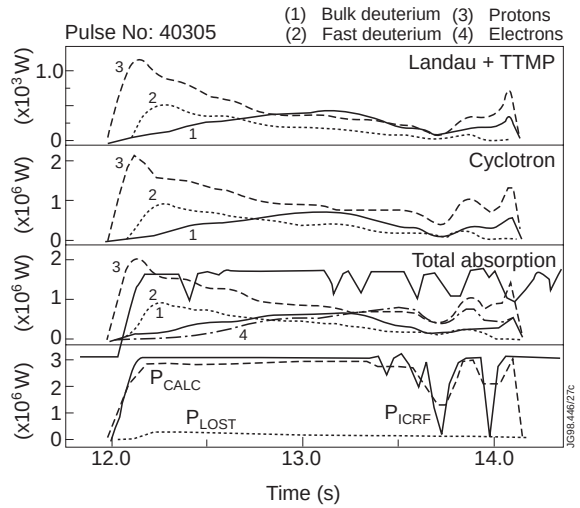

Fig.9: *Power partition between plasma species for JET pulse #40305. At the beginning of the heating phase CD on protons dominates. CD on the NBI deuterons is lower than that on the protons: we attribute this result to the use of polychromatic heating. Ion LD accounts for <1% of total heating, as predicted by theory. Electron heating increases following an increase in T_e due to collisions with fast ions, reaching a maximum absorbed power $P_e \approx 0.7$MW. On the average, a small fraction of power $P_{LOST} \approx 0.2$MW is lost at $r/a>0.9$ due to coupling to low-density surface modes. We observe negligible mode conversion in the plasma centre to ion Bernstein waves (≈0.05MW) and at the plasma edge to electron Bernstein waves (≈0.05MW).*

index at the plasma edge given by $n_{\perp}^2 \approx \varepsilon_{zz}\left(\varepsilon_{xx} - n_{||}^2\right)/\varepsilon_{yy}$. This mode is backward propagating and highly evanescent as the density increases. Coupling to the launched fast wave is locally effected by $Im(n_{\perp H})$, subtracting power to the fast wave at a rate given by $P_{LOST}/P_{ICRF} \approx Im(n_{\perp H})/Re(n_{\perp H})$. From these general results, we conclude that our approach is adequate to describe ICRF wave propagation and absorption in JET deuterium plasmas with minority protons and NBI deuterons.

In fig.9 for #40305 we see that the proton and deuteron slowing-down times are $\tau_p \approx 0.6s$ and $\tau_D \approx 1.1s$: the increase in electron heating is well related to the increase in T_e due to collisions with fast ions. CD on NBI deuterons is lower than on protons: we attribute this result to use of polychromatic heating. During the steady-state heating phase, with $P_{ICRF}=3MW$, we obtain for the fraction of wave power absorbed by electrons, bulk deuterons, NBI deuterons and protons:

In fig.10 for #40474 we see that CD on NBI deuterons is much higher than on protons but for the initial transient phase: we attribute this result to use of monochromatic heating. The fast ion slowing-down times are $\tau_p \approx 0.6s$ and $\tau_D \approx 1.0s$: we relate the increase in electron heating to collisional transfer from fast ions. For the steady-state heating phase, with $P_{ICRF}=5MW$, the fraction of wave power coupled to electrons, bulk deuterons, NBI deuterons and protons are:

$P_e \approx 1.1MW$	$P_{DBULK} \approx 1.0MW$	$P_{DFAST} \approx 1.6MW$	$P_p \approx 1.0MW$
$P_e/P_{ICRF} \approx 22\%$	$P_{DBULK}/P_{ICRF} \approx 20\%$	$P_{DFAST}/P_{ICRF} \approx 32\%$	$P_p/P_{ICRF} \approx 20\%$

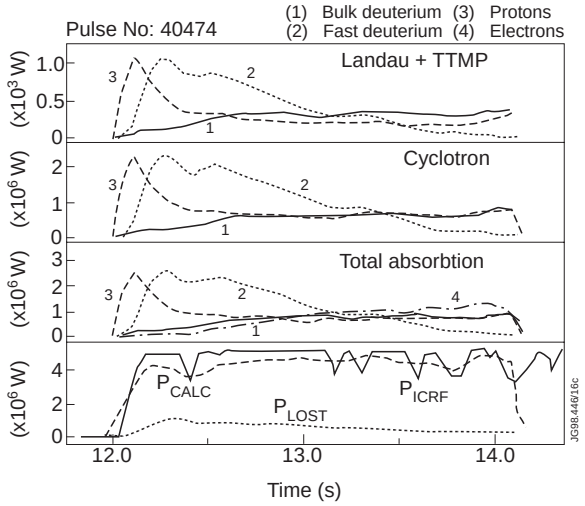

Fig.10: *Power partition between ions and electrons for JET pulse #40474. CD on NBI deuterons is significantly higher than on the protons but during the initial transient phase: we attribute this result to use of monochromatic heating. Ion LD accounts for <1% of total heating, as predicted by theory. Electron heating increases following the increase in T_e due to collisions with fast ions, reaching a maximum absorbed power $P_e \approx 1.4MW$. On the average, a small fraction of power $P_{LOST} \approx 0.3MW$ is lost at the plasma edge due to coupling to low-density surface modes. We observe negligible mode conversion in the plasma centre to ion Bernstein waves (≈0.05MW) and at the plasma edge to electron Bernstein waves (≈0.1MW).*

In fig.11 for #40554 we see that CD on protons is the main heating process during ramp-up of ICRF power, and bulk deuterium heating is important in the steady-state phase. For *t=7.5-7.8* we find mode conversion to Bernstein waves at *0.6<r/a<0.8*, producing predominant electron heating. The fast ion slowing-down times are longer, $\tau_p \approx 1s$ and $\tau_D \approx 1.8s$: this relates well to a slower increase in electron heating. For the steady-state heating phase, with $P_{ICRF}=2MW$, the fraction of wave power absorbed by electrons, bulk deuterons, NBI deuterons and protons are:

$P_e \approx 0.1MW$	$P_{DBULK} \approx 0.8MW$	$P_{DFAST} \approx 0.1MW$	$P_p \approx 0.8MW$
$P_e/P_{ICRF} \approx 5\%$	$P_{DBULK}/P_{ICRF} \approx 40\%$	$P_{DFAST}/P_{ICRF} \approx 5\%$	$P_p/P_{ICRF} \approx 40\%$

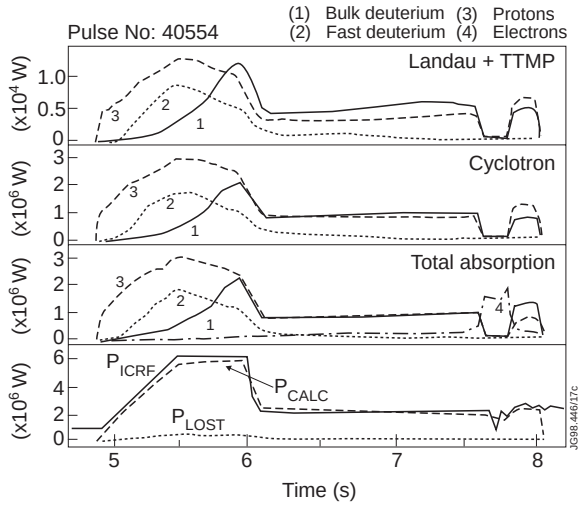

Fig.11: *Power partition between plasma species for JET pulse #40554. At the beginning of the heating phase CD on protons is the dominant absorption process, whereas for the steady-state phase we find significant CD on bulk deuterons. For the plasma conditions of this pulse, the antennae with π/2 phasing ($k_{||}=3m^{-1}$) produce a wave spectrum prone to mode conversion to electron Bernstein waves in the outer region of the plasma, for 0.6<r/a<0.8. This becomes the dominant absorption mechanism at t=7.5-7-8. On the average, a small fraction of power $P_{LOST} \approx 0.2MW$ is lost at the plasma edge due to coupling to surface modes, and we observe negligible mode conversion in the plasma centre to ion Bernstein waves (≈0.05MW).*

Fig.12 shows the perpendicular fast ion energy content for #40305, #40474 and #40554: our results agree quantitatively with magnetic and NPA measurements. Proton heating dominates during the initial transient phase of the heating, and CD on bulk deuterons becomes important only for $T_{DBULK} \geq T_e$ and $n_{DBULK}T_{DBULK} \geq \{n_pT_{\perp p},\ n_{DFAST}T_{\perp DFAST}\}$. We see that $W_{\perp CALC} > W_{\perp MEAS}$: we see this systematic small difference, comparable to the uncertainties of the measurements, but for the initial transient phase of #40554. We attribute this result to the use of a simplified energy balance, neglecting ion-ion collisions and conservation of toroidal angular momentum: thus in our calculations we tend to overestimate the fast ion energy. Inclusion of such effects is beyond the scope of this work, since it would require a considerable effort on the modelling of the NBI deuterium distribution function without adding significantly to its interpretation.

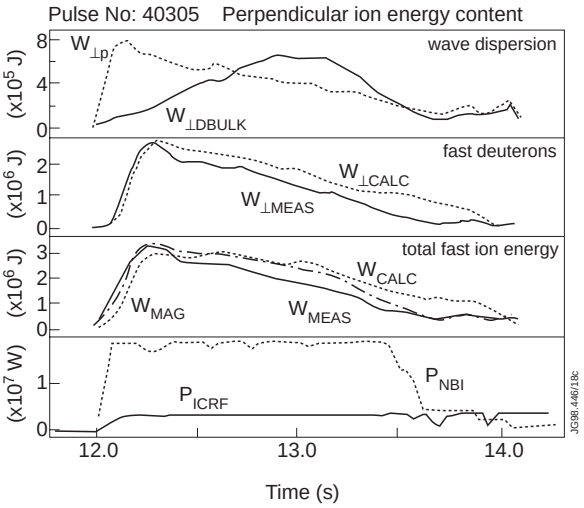

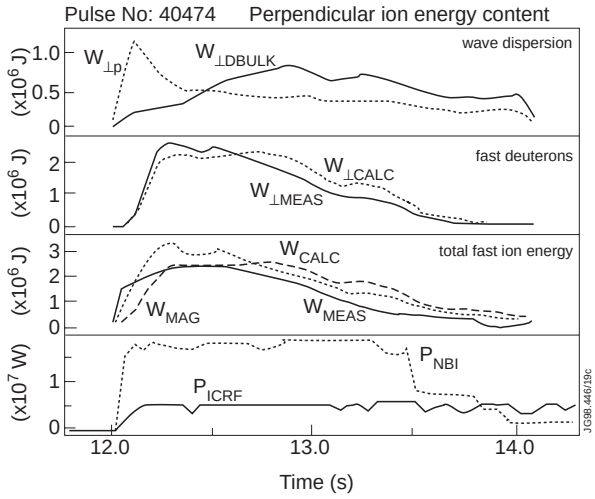

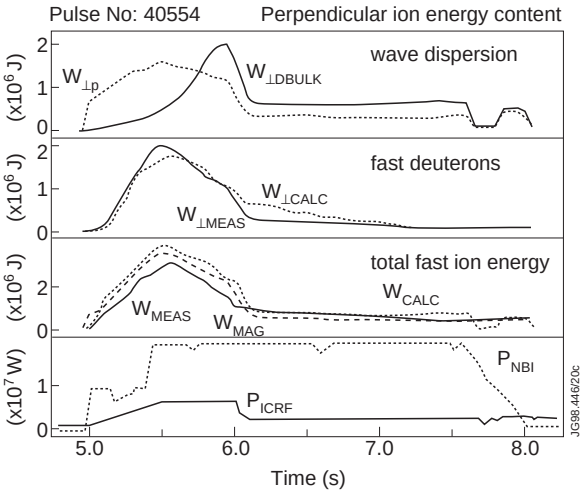

Fig.12: *Perpendicular ion energy content for the pulses analysed here. Our calculations are in quantitative agreement with NPA and magnetic measurements, usually within <15%. The increase in T_{DBULK} due to collisions with NBI deuterons produces stronger absorption of ICRF power, which in turn subtracts wave power to protons and NBI deuterons, determining an increase in the bulk ion energy content. We notice that the calculated perpendicular energy content of NBI deuterons is systematically in excess of ≈15% of that measured by the NPA.*

Fig.13 shows comparison between the perpendicular temperature of NBI deuterons measured by the NPA $T_{\perp NPA}$, the modelled temperature T_{EFF} and that deduced from the fast ion energy $T_{\perp DFAST}$. Using eq.[22] to interpret the magnetic measurements, we deduce a perpendicular temperature using toroidal symmetry, assuming gaussian profiles for the fast ion densities and temperatures with widths λ and δ, considering fixed $T_{||}/T_{\perp}=\alpha$ and normalising W_{MAG} to the fast ion density measured by the NPA. Thus we obtain

$$W_{MAG} = \sum_{FAST} (1+2\alpha)\left(\pi R_0 a^2\right)\sqrt{\pi\beta}\,erf\left(\sqrt{\beta}\right) n_{FAST} T_{\perp FAST} = W_{\perp DFAST} + W_{\perp p} \ .$$

Here a and R_0 are the plasma minor radius and geometric centre, and $\beta=1/\delta+1/\lambda$. We obtain quantitative agreement between these results within the uncertainties of the measurements, usually *15%*. This finally confirms the capability of our approach to interpret experiments with ICRF+NBI heating of deuterium plasmas. We find that T_{EFF} and $T_{\perp DFAST}$ are larger than $T_{\perp NPA}$, which could confirm the need for inclusion of ion-ion collisions and conservation of toroidal angular momentum in modelling the velocity distribution function of NBI deuterons.

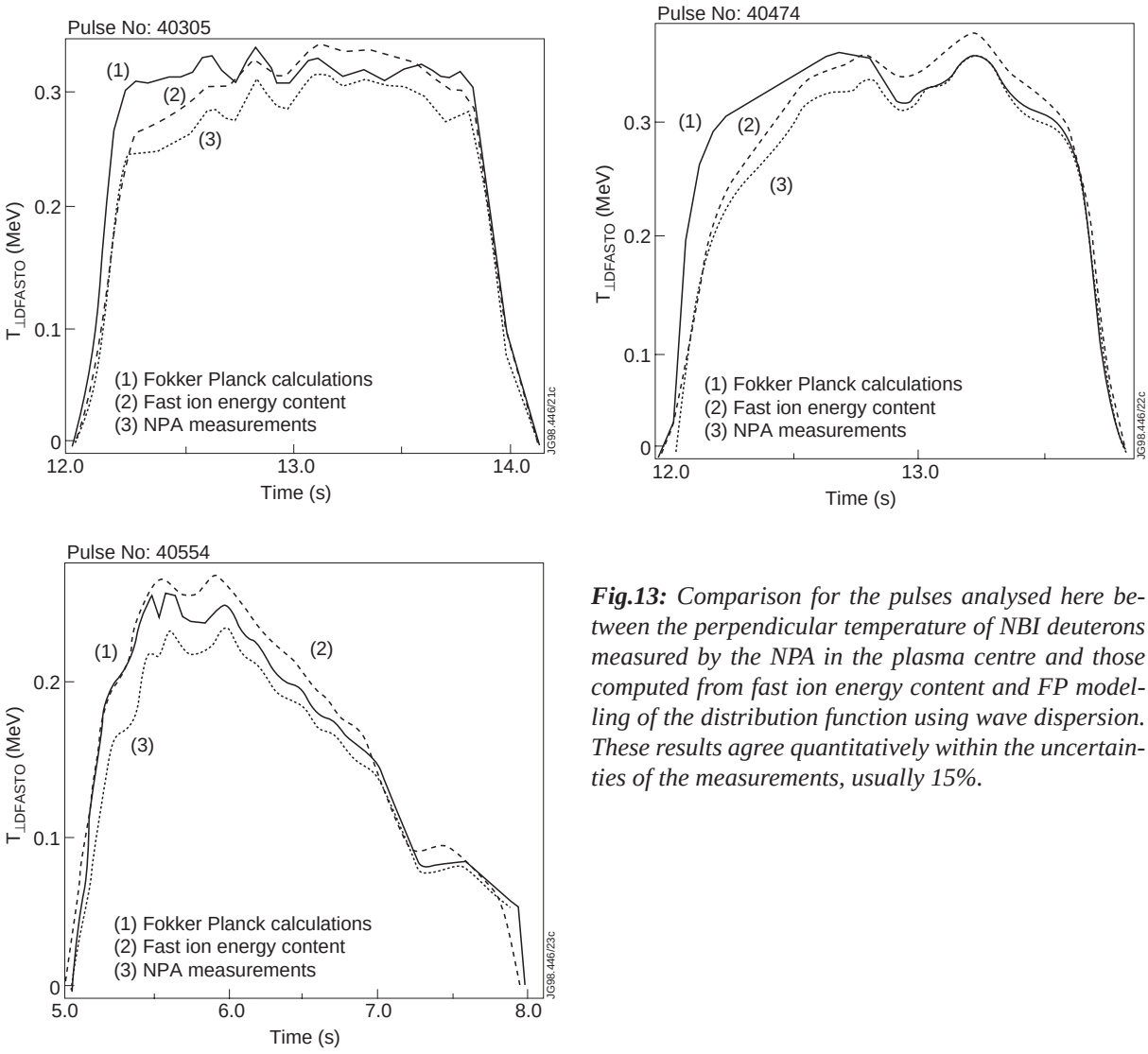

Fig.13: *Comparison for the pulses analysed here between the perpendicular temperature of NBI deuterons measured by the NPA in the plasma centre and those computed from fast ion energy content and FP modelling of the distribution function using wave dispersion. These results agree quantitatively within the uncertainties of the measurements, usually 15%.*

5. DISCUSSION

In this paper we have shown interpretation and modelling of measurements of the distribution function of hydrogen isotope ions during multispecies minority ICRF heating of deuterium plasmas in JET. ICRF power is tuned to central 1st harmonic heating of minority protons. The presence of a second minority resonant species into the plasma, such as the NBI deuterons, causes part of the ICRF power to transfer to 2nd harmonic heating of these supra-thermal ions.

Hot plasma theory allows us to consider thermal and overlapping cyclotron harmonic effects in the analysis of wave propagation by using a complex wavenumber in cylindrical geometry. An iterative method for computing the hot-plasma dispersion relation and power deposition for ICRF waves has been developed for plasmas containing minority anisotropic fast ions using measured thermal majority and non-thermal minority distribution functions as input for the calculations. We solve iteratively the hot-plasma dispersion relation considering electron and hydrogen ion species with their respective concentrations, summing over an appropriate number of cyclotron harmonics to account for the non-local interaction of the ions with the wave

field. We compute collisionless partition of ICRF power between electrons and ions due to CD, LD and TTMP, mode conversion to ion and electron Bernstein waves and parasitic loss of power due to coupling of the launched fast magnetosonic wave to low-density surface modes at the plasma edge. During the initial transient phase of the heating CD on the protons is the dominant absorption process. Collisionless bulk deuterium heating is negligible for $T_{DBULK} \leq T_e$, but increases with the ion temperature and can become significant for $T_{DBULK} > T_e$. Direct electron heating, due to LD+TTMP damping, accounts for $\leq 25\%$ of ICRF power, and increases following the increase in T_e due to collisions with fast ions.

The perpendicular energy content of NBI deuterons and protons deduced from the measured distribution functions and calculated using hot-plasma dispersion relation and ion-electron collisional energy balance is compared with the magnetic measurement. We find quantitative agreement within the uncertainties of the measurements. Finally the measured perpendicular temperature of the NBI deuterons is compared in the plasma centre with those computed from magnetic measurements of the fast ion energy and FP modelling of the distribution function: quantitative agreement is again found within the uncertainties of the measurements.

The computational time required to perform these calculations on the JET IBM 3090 system using a space resolution $\Delta r \approx 3cm$ is typically $\approx 3\text{-}5$ minutes of CPU time per time point with a required numerical accuracy $< 10^{-8}$ on the iterative solution of the wave dispersion relation. Work is now underway to optimise the algorithms used in our numerical procedures.

6. CONCLUSIONS

We have obtained quantitatively self-consistency between NPA measurements of the proton and deuteron distribution functions and modelling of the ICRF-heated ion distribution function by using a complex perpendicular wavenumber in cylindrical geometry for the wave dispersion calculations. Inclusion of ion-ion collisions and conservation of toroidal angular momentum could be required to further improve the accuracy of our model, though at the expense of a considerable effort on the analytical modelling and numerical computation of the ICRF-heated ion distribution function.

Despite the very significant differences between the previous calculations used in JET and those considered here, they both appear to be able to interpret satisfactorily the experiments, thus complementing each other. Moreover, we have demonstrated the necessity for inclusion of power loss at the plasma edge through coupling to low-density surface modes, which was unexplained by the previous JET approach. We conclude that for our purposes the actual magnetic geometry is not of primarily importance, since we are mostly interested in quantities evaluated in the plasma centre, where the effects due to the presence of the poloidal magnetic field are negligible. Conversely, we need to consider the full hot-plasma dispersion relation summing over an appropriate number of cyclotron harmonics to account for the large Larmor radius of the fast ion populations and to model in a phenomenological way the non local interaction between the wave field and the ions.

ACKNOWLEDGEMENTS

The authors would like to thank Professor Malcolm Haines for support and encouragement of this work. We are also indebted to Dr.Chris Lashmore-Davies for clarifying discussion on wave dispersion and absorption, to Terry Martin for help and advise on the numerical solution of the dispersion relation and to Dr.Klaus-Dieter Zastrow for careful analysis of impurity measurements used in this work.

REFERENCES

[1] B.Coppi, S.Cowley, R.Kulsrud, P.Detragiache and F.Pegoraro, *Physics of Fluids **29*** (1986), 4060.

[2] R.B.White, P.H.Rutherford, P.Colestock and M.N.Bussac, *Physical Review Letters* **60** (1988), 2038.

[3] A.A.Korotkov, A.Gondhalekar and A.J.Stuart, *Nuclear Fusion* **37** (1997), 35.

[4] K.G.McClements, R.O.Dendy and A.Gondhalekar, *Nuclear Fusion* **37** (1997), 473.

[5] M.Brambilla, *Computer Physics Reports* **4** (1986), 1.

[6] M.Brambilla and T.Krücken, *Nuclear Fusion* **28** (1988), 1813.

[7] L.G.Eriksson, M.J.Mantsinen F.G.Rimini, F.Nguyen, C.Gormezano, D.F.H.Start and A.Gondhalekar, *JET Report*, JET-P(97)17, 1997.

[8] O.Sauter and J.Vaclavik, *Nuclear Fusion* **32** (1992), 1455.

[9] A.Kay, R.A.Cairns and C.N.Lashmore-Davies, *Plasma Physics and Controlled Fusion* **30** (1988), 471.

[10] C.N.Lashmore-Davies, V.Fuchs, R.A.Cairns and D.C.McDonald, *Proceedings 5th International Atomic Energy Agency Technical Committee Meeting on Alpha Particles in Fusion Research*, JET, Abingdon, UK, 1997.

[11] T.H.Stix, *Nuclear Fusion* **15** (1975), 737.

[12] L.G.Eriksson and T.Hellstein, *Physica Scripta* **52** (1995), 70.

[13] T.H.Stix, *Waves in Plasma*, American Institute of Physics, New York, 1992.

[14] L.G.Eriksson, T.Hellsten and U.Willén, *Nuclear Fusion* **33** (1993), 1037.

[15] J.Wesson, *Tokamaks*, Clarendon Press, Oxford, 1997.

[16] J.Heading, *An Introduction to Phase-Integral Methods*, Wiley, New York, 1962.

[17] D.Testa, *Ph.D.Thesis* 1998, Imperial College of Science, Technology and Medicine, London.